A review of sheet cavitation inception mechanisms

Martijn van Rijsbergen[1]*

ISROMAC 2016

International Symposium on Transport Phenomena and Dynamics of Rotating Machinery

Hawaii, Honolulu

April 10-15, 2016

Abstract

A review is made of the physical mechanisms of sheet cavitation inception. Next to the local pressure, also the characteristics of fluid, solid surface and flow determine the inception process. Five inception mechanisms are described with key parameters such as free-stream nuclei, roughness elements, surface-bound nuclei and a laminar separation bubble. The resulting forms of attached cavitation are designated as spot, finger or patch cavities. However, a detailed description of the nucleation process could not be made due to limitations to the spatial and temporal resolution of the available high-speed observations. Therefore, several hypotheses on the working mechanisms of the nucleation process still exist. In particular, further research is required on the contributions to the nucleation process of turbulent pressure fluctuations, mass transfer, gas expansion, evaporation and diffusion.

Keywords

Sheet cavitation — Inception — Nuclei — Surface roughness — Boundary layer

[1]*Maritime Research Institute Netherlands, The Netherlands*
*__Corresponding author__: m.v.rijsbergen@marin.nl

INTRODUCTION

Sheet cavitation is a thin layer of gas and vapour attached to the leading edge of ship propeller blades, pump rotor blades and turbine runner blades. Its inception depends on a local pressure below the saturated vapour pressure and characteristics of fluid, solid surface and flow, like nuclei content, surface roughness and state of the boundary layer [1]. These characteristics can influence the form and shape of a sheet cavity, and even inhibit its appearance despite a negative pressure. Because these inception effects seem to be more pronounced on model scale than full scale, they are often designated as scale effects.

Engineering measures have been developed in model scale facilities to limit such scale effects. However, as the physical mechanisms of sheet cavitation inception are not fully understood, the limits to the methods applied in scaled experiments are not clear. In model experiments, this may result in isolated patches of cavitation, spots or bubbles instead of a continuous sheet cavity. Fortunately, valuable insights have been obtained since the last comprehensive review on the topic 25 years ago [2] by carefully designed and conducted experiments.

The objectives of this paper are to review the existing knowledge on sheet cavitation inception processes and to define areas for further research. Eventually, this should lead to model scale cavitation tests where sheet cavitation inception occurs as close as possible to the vapour pressure. Such well-controlled model tests can then be used for prediction purposes and to validate and improve computational models.

The cavitation inception process can be described in three stages, from wetted flow, via cavitation inception to limited sheet cavitation. This paper treats the first two stages. In each stage the sensitivities to fluid, surface and flow characteristics are discussed for three basic forms of attached cavitation to be introduced in the next section.

Basic forms of attached cavitation

Figure 1 shows three forms of limited, attached cavitation. These cavities have a limited extent in flow direction—clearly beyond inception—but not yet developed enough to show periodic shedding. They remain attached to the solid surface and are stationary in position as long as the ambient conditions do not change. Limited spanwise extents are shown to clearly distinguish between the forms. Also intermediate forms are often observed.

A sheet cavity is built up of a large series of closely packed spot, finger or patch cavities. A general description is given in this section. The conditions at which they occur are discussed in the following sections.

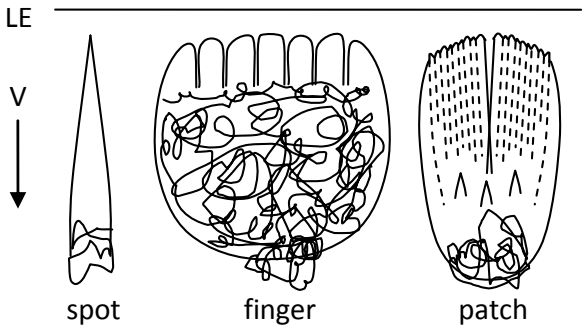

Figure 1. Forms of limited, attached cavitation, flow direction V and relative dimensions/position to the leading edge (LE) not to scale.

The first form is designated as spot cavitation. The upstream part of this wedge-shaped cavity has a smooth surface, whilst the downstream part is rough. The second form is designated as finger cavitation. The upstream part

has a smooth surface with characteristic divots in it and the downstream part shows a rough surface. Spot and finger cavitation have been observed on headforms by Parkin & Kermeen [3], Arakeri & Acosta [4], on foils by Arakeri [5] and Guennoun [6], and on propeller blades by Kuiper [7, 8]. The third form is designated as patch cavitation. It has a rough surface all over with characteristic parallel streaks directed downstream from its leading edge. Patch cavitation has been observed on headforms by Holl & Carroll [9], Kuhn de Chizelle et al. [10] and on foils by Kuiper [11].

1 FLUID, SURFACE AND FLOW ASPECTS

Apart from a pressure requirement, the fluid, surface and flow have to possess other aspects to start the sheet cavitation inception process. The relevant characteristics are introduced in this section for use as building blocks in following sections.

1.1 Fluid characteristics

The most important fluid characteristics for cavitation inception are surface tension, free-stream nuclei content and concentration of dissolved gas. The latter two are discussed, as they can vary significantly in cavitation facilities.

Water contains both microscopic bubbles and particles in a size range between a few and several hundred microns. In general, bubble diameters between 10 and 400 µm are considered as relevant for cavitation inception. In cavitation tunnels, the bubble concentration in this diameter range varies between 0.1 and 10 per cm^3, but in some tunnels concentrations of 100 to 600 per cm^3 have been measured [12-14]. Without a specific control system to regulate the bubble spectrum (size and concentration) in a tunnel, it varies with the dissolved gas content, the pressure in the test section and the running time. Since the bubble generation process is different for each tunnel design, the optimum level of the dissolved gas content ranges from 30 to 80% of the atmospheric saturated value [12, 13]. Measured solid particle concentrations in cavitation tunnels range from 5 to 400 per cm^3 [12-15], but often without a specification of the size range. In many cases the solid particle concentration is orders of magnitude larger than the bubble concentration.

In oceans, bubble concentrations of 1 to 3 per cm^3 are found [13]. The concentration of solid particles larger than 10 µm is 10 to 20 per cm^3 [15, 16].

1.2 Surface characteristics

Jones et al. [17] reviewed a number of experiments that demonstrate the existence of gas cavities on surfaces with microscopic roughness, pits or scratches. Hydrophobic surfaces can trap (sub-) microscopic bubbles upon submersion in water. These sites serve as a source for bubble nucleation at sufficiently large supersaturation of dissolved gas, negative pressures or superheats. The effects of roughness on the flow characteristics are discussed in the following section.

1.3 Flow characteristics

In this section, some flow characteristics relevant to sheet cavitation inception are discussed. Kuiper [7] mentions the possible adverse effects on cavitation inception of bubble screening and the favourable effects of a laminar separation bubble and transition to turbulence.

1.3.1 Bubble screening

If a bubble approaches the leading edge of a foil, it will be forced outward by the high pressure at the stagnation point and drawn towards the surface by the point of minimum pressure. Johnson & Hsieh [18] calculated the trajectories of gas nuclei released close to the dividing streamline just upstream of a two-dimensional half body. They found that the smaller the width of the body, the smaller the maximum bubble diameter that returns to the body upstream of the point of minimum pressure. Furthermore, the lower the free-stream velocity, the larger this critical diameter becomes. This effect is less strong than the effect of size. For example, a critical bubble diameter of 150 µm was found at a free-stream velocity of 7.5 m/s and a body width of 5 mm. Van Rijsbergen & van Terwisga [19] found that the experimentally determined trajectories of free-stream bubbles—approaching the leading edge of a NACA 0015 foil—deviated clearly from calculated streamlines for bubble diameters larger than 190 µm.

1.3.2 Laminar separation bubble

A laminar boundary layer on a foil can separate due to a strong adverse pressure gradient. As a result, the pressure gradient is strongly reduced. Instabilities grow in the separated shear layer, usually followed by transition to turbulence. Turbulent mixing entrains fluid from outside the boundary layer causing it to grow. This increases the pressure again and reattachment occurs when the pressure is approximately equal to that without separation. The recirculation zone between the points of separation and reattachment is designated as the separation bubble.

Arakeri [20] showed that the ratio of the height of the separation bubble to the momentum thickness of the boundary layer at separation decreases from 15 to 5 with increasing Reynolds number on a hemispherical headform. O'Meara [21] found the same trend on an airfoil. The thickness of the separation bubble varied between 2 and 4 times the displacement thickness.

1.3.3 Transition to turbulence

Natural transition starts when Tollmien-Schlichting waves develop in a stable laminar boundary layer with a minimum of external forcing. These linear waves break down into non-linear, 3D instabilities. In the final phase of transition turbulent spots are formed which grow in streamwise and spanwise directions. A fully turbulent flow is formed when these spots merge in spanwise direction.

At model scale, natural transition to turbulence on foils and propeller blades occurs relatively far downstream of the leading edge. Upstream of the point of minimum pressure the transition process is suppressed by the favourable pressure gradient. The transition process is stimulated

downstream of the point of minimum pressure. At the same loading, only an increased Reynolds number can move transition upstream. Kuiper [7] found a shift of the transition region on smooth propeller blades from x/c = 0.6 to 0.3 by increasing the sectional Reynolds number from $5x10^5$ to 10^6.

In a so-called "bypass transition" process, the exponential growth of Tollmien-Schlichting waves is bypassed. The breakdown process is forced by larger disturbances such as free-stream turbulence and surface roughness. Strips of distributed roughness—such as carborundum grains with irregular shapes and a 50% area coverage—are commonly used to trip the boundary layer in engineering applications. Isolated roughness elements with cylindrical, hemispherical or a 3D-hill geometry are used for research purposes. The flow around a roughness element can be characterized by two non-dimensional parameters, i.e., the ratio of the roughness height to the displacement thickness (k/δ) and the roughness Reynolds number ($R_k = kU_k/\nu$), in which U_k is the velocity at the height of the roughness.

Roughness-induced transition to turbulence occurs at the critical roughness Reynolds number, $R_{k,crit}$. Based on several experiments, Kerho & Bragg [22] mention a typical $R_{k,crit}$ value of 600, both for isolated and distributed roughness. This value holds for flat plate boundary layers without pressure gradient and $k/\delta < 1$. Values up to 1500 or higher have been found in conditions with a favourable pressure gradient and $k/\delta > 1$.

1.3.4 Isolated roughness element

Several aspects of the flow around an isolated roughness element can influence the cavitation inception process, such as a local pressure reduction, a laminar separation bubble and transition to turbulence.

Van Rijsbergen & Slot [23] have made steady RANS calculations of the flow around a foil with a 3D roughness element at the point of minimum pressure. The roughness element decreased the minimum pressure coefficient with 60% at a chord Reynolds number of 10^6. This effect decreased with decreasing Reynolds numbers until at Re = 10^4 the effect was negligible.

Kerho & Bragg [22] give a short review of the flow regimes downstream of isolated roughness elements as observed and measured in experiments. At R_k = 160 the flow is laminar without separation. At R_k = 300 – 350, a region of separated flow was observed downstream of the element. Matheis et al. [24] made RANS calculations on a 3D hill and observed a growth of the laminar separation region between R_k = 190 and 330. At R_k = 350 – 450, hairpin vortices are generated in the shear layer on top of the element [22]. At higher R_k values, a turbulent wedge appears with its origin clearly downstream of the element. Turbulent spots are formed within the contours of the wedge. A relatively small increase in R_k moves the origin of the turbulent wedge upstream until it reaches the element at $R_{k,crit}$.

1.3.5 Convective diffusion

Parkin & Kermeen [3] observed the growth of microscopic gas bubbles on the surface of a hemispherical head model. The bubbles were found in a narrow band of locations downstream of the point of minimum pressure. The bubbles grew to a diameter of approximately 100 µm within a few milliseconds after appearance. The growth time was found to be proportional to the calculated local pressure, which remained above the vapour pressure. Together with the milliseconds growth time this excluded vaporous cavitation. Air diffusion in still water would give growth times in the order of seconds. Parkin & Kermeen [25] showed that the diffusion process in flowing water—designated as convective diffusion—is much faster. An acceptable agreement between theory and experiment was found, despite of the simplifications in the model. After reaching their maximum diameter, the bubbles detached from the surface and moved downstream at approximately half the free-stream velocity. No clear explanation could be given for the fixed position during growth and detachment of the bubbles, until the work of Arakeri [20]. He observed a similar growth of bubbles on a hemispherical headform, but only near the point of separation. Furthermore, he noticed that the bubbles became entrained into the free shear layer once the bubble size had become equal to the local separation height.

2 NUCLEATION

Nucleation, i.e., the formation of bubbles, does not occur spontaneously when the fluid is supersaturated with dissolved gas or the pressure decreases below the vapour pressure. The characteristics of impurities in the liquid, a surface in contact with the liquid, or a combination of these two determine the pressure at which bubbles are formed [27]. Three types of this so-called heterogeneous nucleation are described in more detail in the following sections.

2.1 Nucleation by diffusion

Groβ et al. [26] investigated the nucleation process induced by an air-supersaturated laminar flow over air-filled cylindrical pits. The diameter of the pits was between 200 and 800 µm. The liquid was silicone oil at pressures well above the vapour pressure. The nucleation rate increased with the supersaturation rate and with the wall shear stress. A model of the mass flux into the surface-bound nucleus based on shear-enhanced diffusion supported, but did not completely clarify the experimental results. Nucleation rates up to 1000 Hz were found. The size of the detached bubbles was between 10 and 1000 µm and decreased with increasing shear rate.

2.2 Bubble expansion

The rapid growth of a gas bubble is the most investigated nucleation mechanism. A free-stream bubble becomes unstable and starts to grow exponentially if the pressure falls below the Blake threshold pressure [28]. This critical pressure is mainly dependent on the surface tension and the initial diameter. Bubbles at room temperature and atmospheric pressure with initial diameters of 2, 10 and 400 µm have critical pressures of respectively -41 kPa, -3.0 kPa and 2.3 kPa. The dynamic response of a bubble to a low pressure peak can be calculated with the Rayleigh-Plesset

equation [28]. The speed of the initial growth is mainly dependent on inertia, hence larger bubbles grow slower.

Borkent et al. [29] studied the nucleation threshold of bubbles trapped in nanoscopic pits in a surface. They were able to validate the crevice model of Atchley & Prosperetti [30] for cylindrical pits with diameters below 1 µm. The critical pressure of these trapped bubbles was more than 2 times lower than for free bubbles of the same size. Bremond et al. [31] studied the dynamic response of bubbles in cylindrical pits with a diameter of 4 to 20 µm. On this scale, the dynamic growth of these gas pockets could be modelled as hemispheric free bubbles of the same volume.

2.3 Tribonucleation

Hayward [32] investigated the generation of bubbles caused by a rubbing motion between two solid surfaces immersed in water. This nucleation by rubbing was designated as tribonucleation. In a test chamber made of glass, filled with water at room temperature and a negative pressure of 0.15 bar, several solid objects were placed on an inclined wall. Once the objects started to move, a bubble was generated which expanded explosively. The occurrence of nucleation was not dependent on the dissolved gas content. Several materials were found to produce bubbles, a sliding magnet, a fast rolling steel ball and sliding soft silicone rubber. It was presumed that sliding was a critical aspect of tribonucleation. Possibly, the fast rolling steel ball had some finite slip in its contact with the wall.

Washio et al. [33] studied tribonucleation using acrylic glass objects and surfaces immersed in water. Several contact motions such as separation and collision—both normal to the contact surfaces— and sliding were tested at pressures ranging from 0 to 80 kPa. The separating motion—constant acceleration from zero speed—did not cause nucleation. A colliding motion, however, did generate a bubble, but this motion had a larger separation speed. In the sliding motion also nucleation above the vapour pressure was found. The size of the maximum developed cavity increased with decreasing pressure and increasing sliding speed.

Wildeman et al. [34] investigated tribonucleation by sliding a sapphire bead over various surfaces immersed in ethanol. The tests were conducted at atmospheric pressure and 8 K below the boiling temperature of ethanol. A threshold velocity (V) for the formation of a trail of bubbles as a function of the normal force (F) was found. The threshold could be described as $FV = c$, where c depends on the material. For aluminium $c = 9$ µW with V in the order of 1 mm/s and F in the order of 10 mN. Nucleation was also found on silicon, but not on copper or glass. The occurrence of nucleation was not dependent on the dissolved gas content, just as found in [32]. Scanning electron microscopy recordings of the wear tracks showed fracturing on the aluminium surface and plastic deformation on the copper surface. Both aluminium and silicon have a thin, brittle oxide layer on their surfaces. Such a layer is absent on copper.

Various hypotheses for the nucleation by rubbing have been formulated and discussed in [34]. The pressure drop induced by the viscous flow in the space between two separating solid surfaces could not easily explain various nucleation events in low-viscosity liquids, such as water and ethanol. An alternative hypothesis was formulated in which fracturing played a central role. The micro-crack—formed at fracturing—filled with gas and vapour before liquid could enter. The observed force-velocity threshold was interpreted as a combination of generation by fracturing, merging and dissolution of bubbles.

3 ATTACHED CAVITATION INCEPTION

The process of attached cavitation inception depends on the characteristics of the fluid, the surface and the flow. Both the fluid and the surface can provide nuclei. The surface and the flow affect the transport of a free-stream nucleus to the surface. Finally, the form of limited cavitation is determined by the characteristics of the surface and the flow.

Below, five inception mechanisms are described. High-speed film and video observations on micro-scale have enabled a detailed description of the visual phenomena. Limitations to spatial and temporal resolution, however, prevented a detailed view of the instant of nucleation. Hypotheses on the key elements of the nucleation mechanisms are formulated and discussed.

3.1 Free-stream bubble & roughness element

The inception process of a streak cavity, induced by a free-stream gas bubble on an isolated roughness element is shown in [19] and [23]. Three cases with two initial diameters and two cavitation numbers are discussed here. The bubbles expanded gradually as they approached the point of minimum pressure on the foil. This growth was enhanced significantly by the low pressure at the roughness element. Calculations indicated that this pressure was below the critical pressure of the three bubbles. When the bubbles passed the roughness element they generated an attached streak cavity downstream the roughness element. At the largest cavitation number, the bubbles expanded, but did not reach their critical radii. In these cases, the largest bubble generated the largest streak. Subsequently, the bubbles travelled on while oscillating. The continued travel of these nuclei after inception was the reason in [19] to assume that they were made of a liquid such as oil. But in [23] it was shown that their growth followed the Rayleigh-Plesset equation for a gas bubble quite well. At a slightly lower cavitation number, the bubble did grow beyond its critical diameter. A longer streak was generated and the bubble imploded without a clear rebound.

This inception process is characterized by a free-stream bubble which induces a streak cavity but largely keeps its own dynamics (by continuing travelling or imploding). It shows similarities with the travelling bubbles described in Section 3.5. The high-speed video observations of [19] indicated that the location of inception was between the top of the roughness element and approximately 300 µm downstream. This is the region where presumably a laminar separation bubble is present [22, 24]. Instabilities in the thin, free shear layer may promote mass transfer from the passing bubble to the recirculation region as well as

evaporation. This could explain that a larger passing bubble generated a larger initial streak cavity. Figure 2 shows the inception process including the hypotheses.

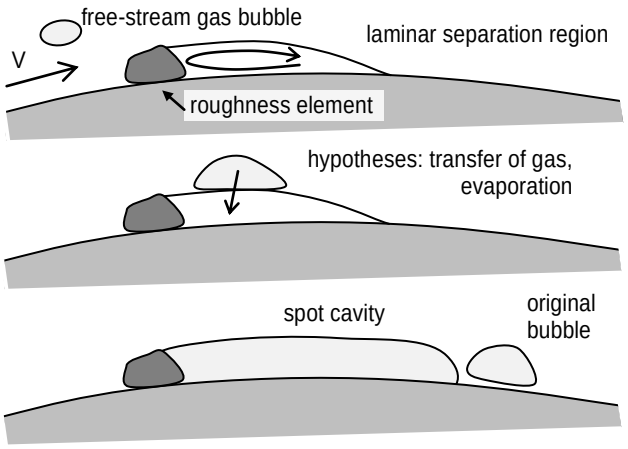

Figure 2. Inception mechanism for a free-stream gas bubble and a roughness element based on [19], flow V from left to right.

3.2 Free-stream particle & roughness element

In [19], a class of free-stream nuclei was identified that induced a stationary cavity on a roughness element, but with clearly different characteristics than a bubble. Their form and diameter remained constant, even after the instant of inception. Their transverse deviations from calculated streamlines were opposite to the deviations of bubbles near the stagnation point and point of minimum pressure. Therefore it was concluded that these nuclei were solid particles.

In the high-speed video observations of [19], where a free-stream particle generated an attached cavity on a roughness element, the particle had a stream-wise displacement of approximately 1 mm per frame. Some frames, however, captured the particle within the optical resolution of 10 µm from the rough surface of the foil. Therefore, it is hypothesized that nucleation occurred at the moment when the particle made contact with a roughness element. This can be designated as tribonucleation, but what is the working mechanism? If the force-velocity relation found in [34] could be extrapolated to velocities in the order of 10 m/s only a normal force in the order of 1 µN would be needed. Alternatively, this relation could be interpreted as the amount of energy needed to produce a bubble. Although this relation describes the observed phenomenon, it does not give a physical explanation. Micro-scale fracturing appears to be an essential physical mechanism in the cases studied in [34] and could also have been present in [19], but it seems not likely in the experiments of [32] because of the smaller forces and softer materials. The collecting and merging of (sub-) micrometer surface nuclei could be an alternative working mechanism. The existence of surface-bound nuclei on the particles or roughness elements—smaller than 10 µm—cannot be excluded on the basis of the high speed images [19].

Once an initial bubble is generated, it probably travels with the particle downstream and causes a cavity in the laminar separation bubble downstream of the roughness element as a free-stream bubble would do, see Figure 3.

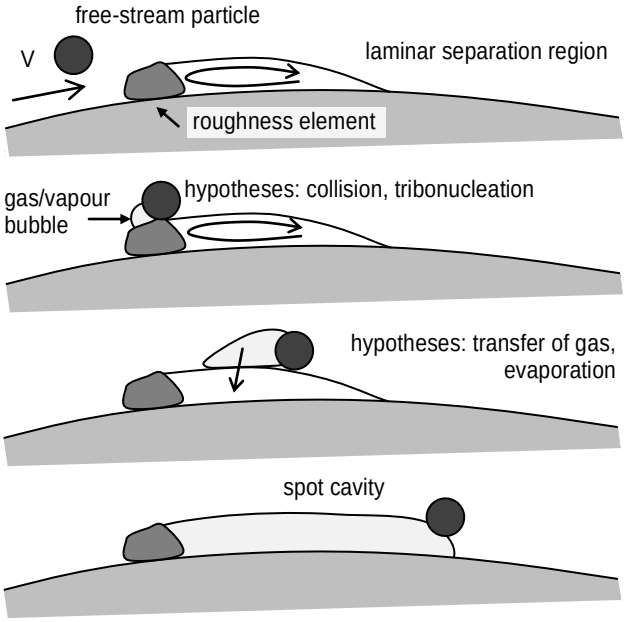

Figure 3. Inception mechanism for a free-stream particle and a roughness element based on [19], flow V from left to right.

3.3 Bubble in surface crevice

Guennoun [6] studied the high-frequency nucleation of bubbles from seemingly arbitrary locations along the line of minimum pressure on a 2D non-polished foil. The average surface roughness was 1 µm. An array of pressure transducers with a 10 mm spacing was mounted in streamwise direction in the foil. The pressure taps with a diameter of 1 mm were smoothly filled with a pressure-sensitive compound. The pressure tap near the point of minimum pressure was found to be a reproducible nucleation site. High-speed micro-scale observations with a resolution of 30 µm could not reveal a surface-bound nucleus. But the high nucleation rate up to 8 kHz indicated that the source of the nuclei was not in the free-stream liquid, but on the surface. A micro-scale crevice in the surface was assumed to stabilize a bubble. The train of travelling bubbles could be changed into spot cavitation by increasing the angle of attack, increasing the Reynolds number or decreasing the cavitation number. The same phenomenon was observed on an elliptic foil. Now, the origin of the travelling bubbles could be traced down to a bubble entrapped by an (unintentional) 50 µm roughness element, just upstream of the point of minimum pressure. On a polished foil with an average surface roughness of 0.2 µm only finger-type cavitation patches were observed.

The experimental results in [6] and [35] indicated two spot cavitation inception mechanisms. At a fixed rate of pressure decrease, either a trail of travelling bubbles gradually merged into a spot or, a delay in nucleation was followed by a fast growth of a single bubble into a spot. Spot cavitation inception from a trail of travelling bubbles occurred mostly at small angles of attack, see Figure 4.

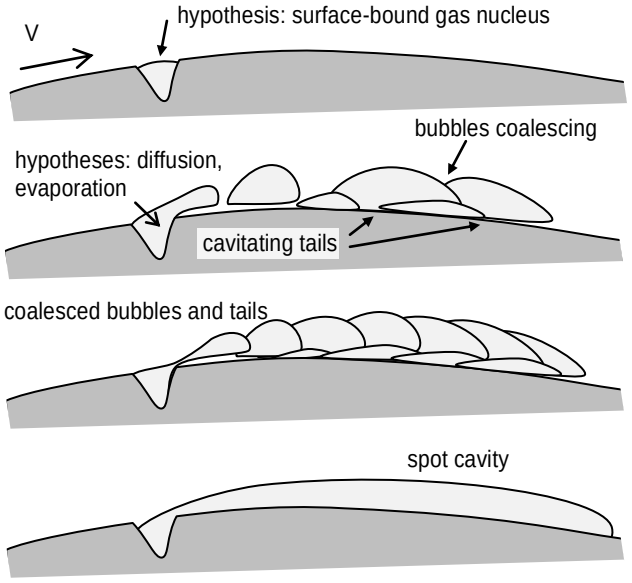

Figure 4. Inception mechanism for a surface-bound bubble at a small angle of attack based on [6, 35], flow V from left to right.

A decrease of the ambient pressure increased the nucleation rate and the size of the bubbles. The bubbles began to merge with each other, first at the end of the trail and then at the start. Almost simultaneously, the process of attachment to the surface began. Cavitating tails and transient patches upstream of the travelling bubbles— see Figure 7—were observed at the end of the trail. Again, this process starts at the end of the trail and moves upstream with increasing nucleation rate. The process of attachment is supported by pressure measurements. Near the nucleation site, negative surface pressures were measured when a bubble passed. This indicates that the bubbles were separated from the surface by a thin layer of liquid. Upstream of a travelling bubble, the pressure decreased, increased and decreased again. This was interpreted as a signature of a 3D boundary layer separation.

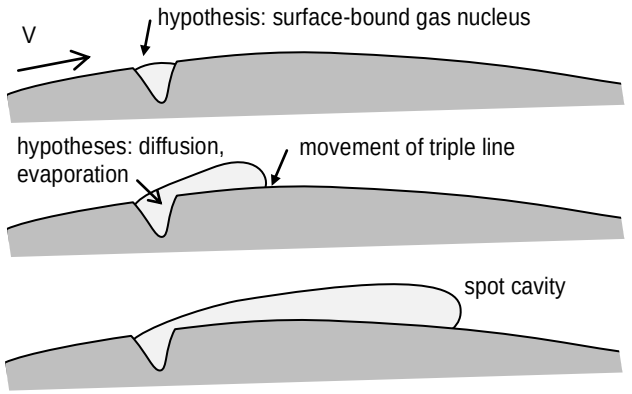

Figure 5. Inception mechanism for a surface-bound bubble at a large angle of attack based on [6, 35], flow V from left to right.

Attached cavitation inception by the growth of a single surface-bound bubble occurs primarily at large angles of attack, see Figure 5. Two events have been reported where the downstream edge of a pressure tap served as a nucleation site. Before inception, the pressure could be decreased to -20 kPa and -48 kPa respectively. After inception the pressure increased to approximately -15 kPa. The liquid at the tap upstream of the nucleation site was clearly under tension. The pressure did not reach the vapour pressure after inception, because the tap was only marginally covered by gas and vapour. After inception—with a limited cavity on the foil—the pressure downstream of the cavity increased to a value above that in the wetted flow. This indicates the presence of a reattachment point [9]. When the ambient pressure was decreased further, the cavity length increased and the surface pressure decreased down to the vapour pressure as soon as the sensor was covered by the cavity.

On a number of occasions, travelling bubbles were observed at one nucleation site and spot cavitation at a neighbouring site. Also large differences in nucleation rate at two neighbouring nucleation sites were observed. This indicated that local phenomena such as the initial volume of gas, the local flow and interfacial forces between liquid, solid and gas play a significant role in the nucleation process.

Guennoun et al. [35] suggested vaporization from a gas inclusion as the primary working mechanism of nucleation from a surface. The non-condensable gas only served as a catalyst for the vaporization and would remain largely in the crevice after detachment of a bubble. The nucleation models in [29] and [31], however, assume that expansion of non-condensable gas is the main feature. The constant vapour pressure term in their model implicates a minor contribution of the vapour production. Using the model of [31], the size of the surface-bound nuclei in the two events of spot cavitation inception mentioned above can be estimated to be 2 to 3 µm. Diffusion could play a significant role in the nucleation process by providing a continuous influx of non-condensable gas into the surface-bound nucleus, as discussed in [26]. It is mentioned several times in [6], but eventually neglected in the modelling of nucleation.

3.4 Free gas bubble & laminar separation region

Cavitation inception on a body with a laminar separation bubble occurs first as travelling bubbles in the reattachment zone, far downstream of the point of minimum pressure. Two cases of travelling bubble cavitation inception have been reported by Parkin & Kermeen in [3] and [25] and were further interpreted by Arakeri [20]. The inception process follows on the growth and detachment of microscopic bubbles as described in Section 1.3.5.

After travelling a few millimetre in the free shear layer, the bubbles arrived in the transition region where they grew explosively to many times their original size in less than 0.2 ms and travelled on. The growth rate indicated vaporous cavitation, but the expansion occurred in a region with a higher mean pressure. Furthermore, some bubbles passed the zone without expanding. Therefore, it was suggested in [25] and [20] that strong pressure fluctuations in the transition region could decrease the local pressure below the vapour pressure. Katz [36] measured wall pressure fluctuations with peak amplitudes up to 18% of the dynamic head in the reattachment zone. The measured characteristic

periods in the order of 1 ms would be sufficient to expand bubbles with diameters up to 200 µm. As the pressure is further decreased, attached finger-type (a.k.a. band) cavities are observed with a leading edge closer to the point of separation [20]. Katz [36] noticed that the transition from travelling bubble cavitation to attached band cavitation occurs very rapidly. The process starts at some point—at the same axial location—and expands laterally. He suggests that this process is induced by bubbles that are swept by the reverse flow to the stable part of the separation zone. The inception process—including hypotheses—is shown in Figure 6.

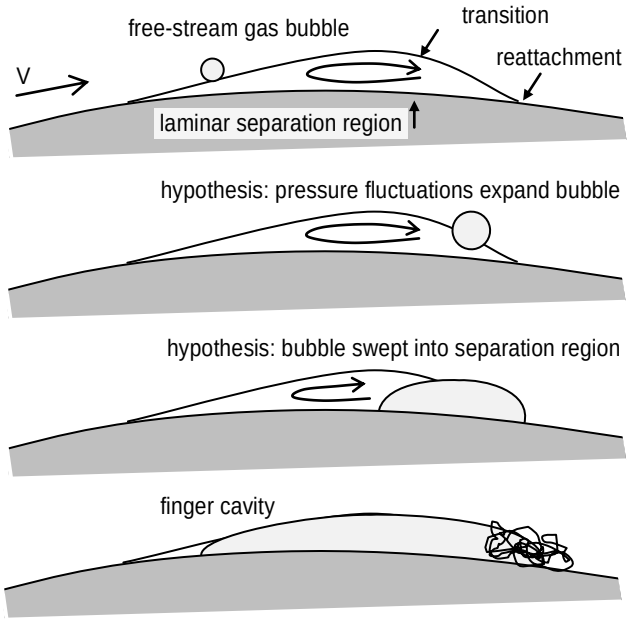

Figure 6. Inception mechanism for a free gas bubble and a laminar separation region based on [20, 37], flow V from left to right.

3.5 Travelling bubble & boundary layer

Li & Ceccio [37] examined the generation of attached cavities by travelling bubbles on a hydrofoil. Small bubbles were generated upstream of the leading edge of the foil which expanded while travelling over the tension region, see Figure 7.

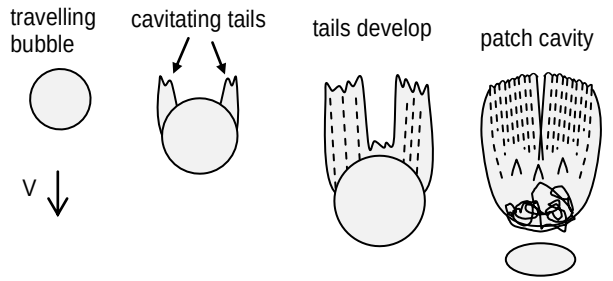

Figure 7. Inception process for a travelling bubble and a laminar boundary layer based on [10, 36], flow V from top to bottom.

The spherical bubbles deformed to hemispherical 'caps' if the distance to the surface was approximately equal to the boundary layer thickness. With a laminar boundary layer on the foil, two cavitating 'tails' were formed at the lateral sides of a bubble. These attached patches of cavitation grew in span-wise and chord-wise direction as the bubble travelled on and connected to each other at the symmetry line. Finally, the bubble detached from the patch cavity and travelled on while the patch cavity remained.

The laminar boundary layer was considered susceptible to transition, because of the relatively high Reynolds number (1.24×10^6) and an adverse pressure gradient. Velocity fluctuation measurements in the boundary layer upstream of the travelling bubbles, i.e. in their wake, showed that transition to turbulence was stimulated by the bubbles. This complies with the dye visualizations of Briançon-Marjollet et al. [38]. Kuhn de Chizelle et al. [10] observed the development of similar patches on a range of headforms. The occurrence of patch cavities increased with the size of the headform, a larger velocity and a smaller cavitation number. In a turbulent boundary layer, a more chaotically formed patch of cavitation was generated by travelling bubbles [37]. There were no clear tails observed and the patch did not persist after passage of the bubble.

In [37] it was hypothesized that the travelling bubbles squeezed the boundary layer and generated streamwise vorticity which induced two turbulent spots on the spanwise edges of the bubble. These spots may lead to a local 3D boundary layer separation and fill with vapour supplied by the bubble. In the wetted flow, however, no boundary layer separation was measured. Maybe first evaporation at the surface occurs, followed by boundary layer separation [39]. Alternatively, it was suggested that the turbulent spots could stimulate previously sub-critical surface nuclei to form attached cavities. The patch cavities in [9] and [10] do bear some resemblances with dye visualisations of turbulent spots by Gad-el-Hak et al. [40]. The upstream part contains streamwise streaks and the downstream part is more turbulent.

4 SENSITIVITY STUDIES

The effects of nuclei and turbulence on sheet cavitation inception as found in sensitivity studies are discussed in this section.

4.1 Nuclei

The review of mechanisms above has shown the essential role of nuclei for attached cavitation inception. In this section several aspects of nuclei, such as the type, origin, size range and concentration are discussed.

Keller [41] studied the effect of the free-stream nuclei spectrum on cavitation inception on various headforms. The surfaces were polished, resulting in a maximum roughness of 0.1 µm. This minimized the size of surface-bound nuclei. Degassing and filtering the water decreased the concentration of nuclei (solid and gaseous) by 35% and 95%, respectively. Degassing and filtering the water significantly lowered the cavitation inception number (σ_i). This could hold for attached or bubble cavitation since the type of incipient cavitation was not specified. Presumably, degassing also decreased the maximum bubble diameter, thus decreasing the critical pressure of the largest bubble

and increasing the tensile strength of the water. The effect of filtering was interpreted by Keller as a confirmation of the nucleus model of Harvey, i.e., gas trapped in small crevices of hydrophobic particles. Alternatively, it could support the tribonucleation mechanism, see Section 2.3.

Gindroz & Billet [42] found a significant decrease of σ_i with an increase of the tensile strength of the water for bubble and tip vortex cavitation on propeller models. Only a minor decrease in σ_i was found for sheet cavitation. Apparently, the sheet cavitation inception process is less dependent on the critical pressure of free-stream bubbles than the inception processes of bubble and tip vortex cavitation. Either the expansion of free-stream bubbles is not essential in the sheet cavitation inception process or the expansion of surface-bound nuclei dominate the inception process in this case. Mées et al. [12] found nearly 20 times more solid than gas nuclei in the same facility. This could indicate a prominent role for solid nuclei (tribonucleation) in the inception process.

Noordzij [43] found that sheet cavitation was suppressed on smooth propeller blades in MARIN's Depressurized Towing Tank (DTT). Free-stream bubbles established a fully developed sheet on all blades in one case but in another case only some additional spot cavities were observed. Kuiper [7] found a very limited improvement by seeding free-stream bubbles upstream of a smooth propeller model in the DTT. With leading edge roughness on the propeller blades, however, a fully developed sheet cavity was observed. Free-stream bubbles could not further improve the extent of the cavity.

Van Rees et al. [44] obtained a good agreement between the pressure side sheet cavity on a propeller with leading edge roughness in MARIN's cavitation tunnel at a standard air content and in the DTT with nuclei seeding. Without seeding no cavitation was observed. This seemed in contradiction with the findings of Kuiper. Therefore, Van Rijsbergen & van Terwisga [45] investigated the same propeller model as used by Kuiper with leading edge roughness on the blades in the DTT. Only a few spots were observed without seeding at lower propeller loadings. By increasing the free-stream nuclei content, the number of spots increased until a fully developed sheet was formed. The sheet cavity was almost completely developed without nuclei seeding at higher propeller loadings. Seeding fully closed the sheet cavity.

In [1, 5, 7] wedge-shaped spots of bubble cavitation were observed at mid-chord positions. In most cases the origin of the bubbles could be traced back to a roughness element or small surface imperfections at the leading edge of the foil or propeller blade. In [7] it was hypothesized that microscopic, turbulent low-pressure regions at the roughness elements caused dissolved gas in the water to come out of solution which formed free gas bubbles. A minimum roughness height to boundary layer thickness ratio and locally supersaturated water were assumed to be critical parameters. The same mechanism was assumed to occur for sheet cavitation inception—when the roughness elements were located in the minimum pressure region. A surface-bound nucleus as observed in [6] at a roughness element on an elliptic foil may be the connecting element between diffusion and production of free gas bubbles. The generation of separate bubbles at small angles of attack and attached spot cavitation at large angles of attack corresponds with the findings in [6]. In [45] the presence of small remnant free-stream nuclei is suggested. A lower minimum pressure on the blades could expand smaller nuclei at higher propeller loadings. Measurements of the free-stream nuclei spectrum and the leading edge roughness topology could provide more definitive explanations for these findings.

Surface-bound nuclei—provided by gas trapped in micro-scale pits—offer a controllable way of attached cavitation inception [31]. The size of these pits need to be as large as possible to generate a spot cavity just below the vapour pressure. If the size is too large, however, bubbles will be generated above the vapour pressure [26]. The production of pits in the double-curved surfaces of the leading edge of a blade is challenging but there are several advantages. Contrary to distributed roughness, the pits have a minimal disturbance of the boundary layer. Furthermore, seeding of free-stream nuclei is no longer required which improves the quality of noise measurements [46].

4.2 Turbulence

It is commonly assumed that the boundary layer is fully turbulent at full scale which will enhance cavitation inception. Therefore, the effect of turbulence—either in the free-stream or generated by roughness—on sheet cavitation inception has been investigated on model scale.

In [7] paint tests and cavitation tests were carried out on propeller models with two grain sizes of distributed leading edge roughness, 30 and 60 μm. The paint tests with the 30 μm roughness showed that the boundary layer was often not turbulent. Furthermore, no cavitation was found when the boundary layer was not tripped. With 60 μm roughness both a turbulent boundary layer and cavitation was observed. Therefore, it was hypothesized that cavitation inception on the roughness elements only occurs when the roughness induces a turbulent boundary layer. However, at a propeller Reynolds number of 10^6, k = 60 μm and r/R = 0.5, R_k is approximately 430. Because this value is clearly below $R_{k,crit}$, this may indicate a transition further downstream. Paint tests typically lack information near the leading edge due to the high speeds. This might have masked the exact chordwise position of transition.

Ligtelijn et al. [46] presented a diagram—based on systematic propeller model cavitation inception tests—to determine the appropriate roughness size as a function of the sectional Reynolds number. The corresponding R_k values are all well below $R_{k,crit}$. Furthermore, in [45] cavitation inception was found at roughness elements with R_k = 210. These experiments indicate that turbulence at the roughness elements may not be a requirement for cavitation inception. However, the R_k values may be sufficiently high to generate a laminar separation bubble at the roughness element. The correlation with turbulence far downstream may indicate that instabilities are already present in the free shear layer.

The effect of free-stream turbulence on cavitation inception on roughened propellers was investigated in [44]. Two propellers were tested at free-stream turbulence intensities of approximately zero (without grid) and 1% (with grid). No effect was found on the radial cavitation extent of one propeller. The other propeller showed a significant increase in cavitation extent. In the latter case, however, the grid was probably cavitating and thus generating free-stream nuclei. The effect of free-stream turbulence and leading edge roughness on cavitation inception was investigated by Korkut & Atlar [47]. An increase of the free-stream turbulence intensity from 3.3 to 4.5% increased σ_i for sheet cavitation on smooth propeller blades. A similar increase was found for an increase of the leading edge roughness grain size. It was hypothesized that free-stream turbulence has a similar effect on the boundary layer as leading edge roughness. Alternatively it was suggested that the used wire meshes not only generated free-stream turbulence but also free-stream nuclei. In the tests with the roughened propeller blades the roughness may have provided surface-bound nuclei.

More systematic research on the effect of parameters such as k/δ, R_k and pressure gradient on sheet cavitation inception is necessary to find the exact working mechanism.

5 CONCLUSIONS AND RECOMMENDATIONS

Sheet cavitation inception occurs when the local pressure is below the vapour pressure, gas and vapour dewet the surface and expand at a fixed location. If the free-stream flow provides the necessary nuclei, these need to be brought to the surface first. Surface roughness, a laminar separation bubble and turbulence enhance this process and may compensate for the screening effect. Second, the gas and vapour from the travelling bubble have to come into contact with the surface. It is hypothesized that mass transfer by shear, turbulent mixing and evaporation govern this step in the inception process. A free-stream particle has to make contact with the surface to generate a gas bubble. Roughness elements protruding the boundary layer increase the probability of contact. After advection with the flow, the generated gas bubble can induce attached cavitation just like a free-stream bubble. A surface-bound nucleus can generate an attached cavity without a laminar separation bubble. It is hypothesized that diffusion and evaporation enable this process. Finally, an attached cavity can remain at a fixed location by flow separation, either already present in the wetted flow or generated by the cavity.

High-speed micro-scale observations at increased temporal and spatial resolutions are needed to further narrow down the location of attached cavitation inception and the mechanisms involved. Experiments above and below the vapour pressure and modelling of the of mass transport, diffusion and evaporation are recommended to distinguish between their contributions to the cavitation inception process.

Gas trapped in micro-scale pits are a promising nucleation source in model scale tests. More research on the optimum size of these pits and their production at the leading edge of a blade is necessary.

Leading edge roughness may enable cavitation inception from surface-bound nuclei and from free-stream nuclei. A laminar separation bubble downstream of the roughness elements enhances both processes. Measurements of the free-stream nuclei spectrum and the leading edge roughness topology are recommended to distinguish between the two sources in model scale experiments. It is recommended to investigate the contribution of turbulence to attached cavitation inception by systematic research on the effect of the ratio of the roughness height to the displacement thickness, the roughness Reynolds number and pressure gradient on attached cavitation inception.

REFERENCES

[1] J. H. J. van der Meulen and Y. P. Ye, “Cavitation inception scaling by roughness and nuclei generation,” in *14th Symposium on Naval Hydrodynamics*, 1982.

[2] E. P. Rood, “Review—mechanisms of cavitation inception,” *J. Fluids Eng.*, vol. 113, no. 2, pp. 163–175, Jun. 1991.

[3] B. R. Parkin and R. W. Kermeen, “Incipient cavitation and boundary layer interaction on a streamlined body,” California Institute of Technology, Pasadena, California USA, 1953.

[4] V. H. Arakeri and A. J. Acosta, “Cavitation inception observations on axisymmetric bodies at supercritical Reynolds numbers,” *J. Ship Res.*, vol. 20, no. 1, pp. 40–50, 1976.

[5] V. H. Arakeri, “Water tunnel investigations of scale effects in cavitation detachment from smooth slender bodies and characteristics of flow past a bi-convex hydrofoil,” California Institute of Technology, Pasadena, California USA, 1971.

[6] F. Guennoun, “Étude physique de l’apparition et du développement de la cavitation sur une aube isolee,” PhD Thesis, École Polytechnique Fédérale de Lausanne, 2006.

[7] G. Kuiper, “Cavitation inception on ship propeller models,” PhD Thesis, Delft University of Technology, 1981.

[8] G. Kuiper, “Cavitation and new blade sections,” in *Cavitation and Gas-Liquid Flow in Fluid Machinery and Devices*, 1994, pp. 25–32.

[9] J. W. Holl and J. A. Carroll, “Observations of the various types of limited cavitation on axisymmetric bodies,” *J. Fluids Eng.*, vol. 103, pp. 415–424, 1981.

[10] Y. Kuhn de Chizelle, S. L. Ceccio, and C. E. Brennen, “Observation and scaling of travelling buble cavitation,” *J. Fluid Mech.*, vol. 293, pp. 99–126, 1995.

[11] G. Kuiper, “Effects of Artificial Roughness on Sheet Cavitation,” in *Institute of Mech. Eng., 2nd Conference on Cavitation*, 1983.

[12] L. Mées, D. Lebrun, D. Allano, F. Walle, Y. Lecoffre, R. Boucheron, and D. Fréchou, “Development of interferometric techniques for nuclei size measurement in cavitation tunnel,” in *28th Symposium on Naval Hydrodynamics*, 2010.

[13] M. L. Billet, “Cavitation nuclei measurements - a review,” in *Cavitation and Multiphase Flow Forum*, 1985.

[14] H. J. Heinke, C. Johannsen, W. Kroger, P. Schiller, and E. A. Weitendorf, “On cavitation nuclei in water tunnels,” in *8th International Symposium on Cavitation*, 2012, pp. 407–413.

[15] E. Ebert, A. Kleinwächter, R. Kostbade, and N. Damaschke, “Interferometric particle imaging for cavitation nuclei characterization in cavitation tunnels and in the wake flow,” in *17th International Symposium on Applications of Laser Techniques to Fluid Mechanics*, 2014.

[16] T. J. O'Hern, "Cavitation inception scale effects: Nuclei distributions in natural waters, Cavitation inception in a turbulent shear flow," California Institute of Technology, 1987.

[17] S. F. Jones, G. M. Evans, and K. P. U. Galvin, "Bubble nucleation from gas cavities - a review," *Adv. Colloid Interface Sci.*, vol. 80, pp. 27–50, 1999.

[18] V. E. Johnson and T. Hsieh, "The influence of the trajectories of gas nuclei on cavitation inception," in *6th Symposium on Naval Hydrodynamics*, 1966, pp. 163–179.

[19] M. X. van Rijsbergen and T. J. C. van Terwisga, "High-speed micro-scale observations of nuclei-induced sheet cavitation," in *3rd International Cavitation Forum*, 2011.

[20] V. H. Arakeri, "Viscous effects in inception and development of cavitation on axi-symmetric bodies," PhD Thesis, California Institute of Technology, 1973.

[21] M. M. O'Meara and T. J. Mueller, "Experimental determination of the laminar separation bubble characteristics of an airfoil at low Reynolds numbers," in *4th Fluid Mechanics, Plasma Dynamics and Lasers Conference*, 1986.

[22] M. F. Kerho and M. B. Bragg, "Airfoil boundary-layer development and transition with large leading-edge roughness," *AIAA J.*, vol. 35, no. 1, pp. 75–84, 1997.

[23] M. X. van Rijsbergen and J. Slot, "Bubble-induced sheet cavitation inception on an isolated roughness element," in *9th International Symposium on Cavitation*, 2015.

[24] B. D. Matheis, W. W. Huebsch, and A. P. Rothmayer, "Separation and unsteady vortex shedding from leading edge surface roughness," in *RTO AVT Specialists Meeting*, 2004.

[25] B. R. Parkin and R. W. Kermeen, "The roles of convective air diffusion and liquid tensile stresses during cavitation inception," in *IAHR Symposium on Cavitation and Hydraulic Machinery*, 1963.

[26] T. F. Groß, G. Ludwig, and P. F. Pelz, "Experimental and theoretical investigation of nucleation from wall-bounded nuclei in a laminar flow," in *International Symposium on Transport Phenomena and Dynamics of Rotating Machinery*, 2016.

[27] F. Caupin and E. Herbert, "Cavitation in water: a review," *Comptes Rendus Phys.*, vol. 7, pp. 1000–1017, 2006.

[28] C. E. Brennen, *Cavitation and bubble dynamics*. Oxford University Press, 1995.

[29] B. M. Borkent, S. Gekle, A. Prosperetti, and D. Lohse, "Nucleation threshold and deactivation mechanisms of nanoscopic cavitation nuclei," *Phys. Fluids*, vol. 21, no. 10, p. 102003, 2009.

[30] A. A. Atchley and A. Prosperetti, "The crevice model of bubble nucleation," *J. Acoust. Soc. Am.*, vol. 86, no. 3, pp. 1065–1084, 1989.

[31] N. Bremond, M. Arora, S. M. Dammer, and D. Lohse, "Interaction of cavitation bubbles on a wall," *Phys. Fluids*, vol. 18, no. 12, pp. 1–10, 2006.

[32] A. T. J. Hayward, "Tribonucleation of bubbles," *Brit. J. Appl. Phys.*, vol. 18, no. 5, pp. 641–644, May 1967.

[33] S. Washio, S. Takahashi, K. Murakami, T. Tada, and S. Deguchi, "Cavity generation by accelerated relative motions between solid walls contacting in liquid," *Proc. Inst. Mech. Eng. Part C J. Mech. Eng. Sci.*, vol. 222, no. 9, pp. 1695–1705, Sep. 2008.

[34] S. Wildeman, H. Lhuissier, C. Sun, D. Lohse, and A. Prosperetti, "Tribonucleation of bubbles," *Proc. Natl. Acad. Sci. USA*, vol. 111, no. 28, pp. 10089–94, 2014.

[35] F. Guennoun, M. Farhat, Y. A. Bouziad, F. Avellan, and F. Pereira, "Experimental investigation of a particular travelling bubble cavitation," in *5th International Symposium on Cavitation*, 2003.

[36] J. Katz, "Cavitation phenomena within regions of flow separation," *J. Fluid Mech.*, vol. 140, pp. 397–436, 1984.

[37] C.-Y. Li and S. L. Ceccio, "Interaction of single travelling bubbles with the boundary layer and attached cavitation," *J. Fluid Mech.*, vol. 322, pp. 329–353, 1996.

[38] L. Briançon-Marjollet, J. P. Franc, and J. M. Michel, "Transient bubbles interacting with an attached cavity and the boundary layer," *J. Fluid Mech.*, vol. 218, pp. 355–376, 1990.

[39] M. Hoekstra and G. Vaz, "The partial cavity on a 2D foil revisited," in *7th International Symposium on Cavitation*, 2009, no. 43.

[40] M. Gad-El-Hak, R. F. Blackwelderf, and J. J. Riley, "On the growth of turbulent regions in laminar boundary layers," *J. Fluid Mech.*, vol. 110, pp. 73–95, 1981.

[41] A. P. Keller, "Investigations concerning scale effects of the inception of cavitation," in *Conference on Cavitation, Institute of Mechanical Engineers*, 1974, pp. 109–119.

[42] B. Gindroz and M. L. Billet, "Influence of the nuclei on the cavitation inception for different types of cavitation on ship propellers," *J. Fluids Eng.*, vol. 120, no. 1, pp. 171–178, Mar. 1998.

[43] L. Noordzij, "Some Experiments on Cavitation Inception with Propellers in the NSMB Depressurized Towing Tank," *Int. Shipb. Prog.*, vol. 23, no. 265, 1976.

[44] W. M. van Rees, M. X. van Rijsbergen, G. Kuiper, and T. J. C. van Terwisga, "An exploratory investigation of cavitation inception on the pressure side of propellers," in *ASME Fluids Engineering Division Summer Meeting*, 2008.

[45] M. X. van Rijsbergen and T. J. C. van Terwisga, "Water quality effects on sheet cavitation inception on a ship propeller model," in *7th International Conference on Multiphase Flow*, 2010.

[46] J. T. Ligtelijn, J. van der Kooij, G. Kuiper, and W. van Gent, *Research on propeller-hull interaction in the depressurized towing tank*. MARIN Jubilee Meeting (Hydrodynamics: Computation, Model Tests and Reality), Wageningen, The Netherlands, 1992.

[47] E. Korkut and M. Atlar, "On the importance of the effect of turbulence in cavitation inception tests of marine propellers," *Proc. R. Soc. A Math. Phys. Eng. Sci.*, vol. 458, no. 2017, pp. 29–48, 2002.